

Edge dependence of the supercurrent in the quantum Hall regime

Seong Jang¹, Geon-Hyoung Park¹, Kenji Watanabe², Takashi Taniguchi³ and Gil-Ho Lee^{1,*}

¹ Department of Physics, Pohang University of Science and Technology, Pohang, 37673, Republic of Korea,

² Research Center for Functional Materials, National Institute for Materials Science, Tsukuba, 305-0047, Japan

³ International Center for Materials Nanoarchitectonics, National Institute for Materials Science, Tsukuba, 305-0047, Japan

ABSTRACT

The observation of Josephson current in the quantum Hall regime has attracted considerable attention, revealing the coexistence of two seemingly incompatible phases: the quantum Hall and superconducting states. However, the mechanism underlying the Josephson current remains unclear because of the observed $h/2e$ magnetic interference period and absence of precisely quantized Hall plateaus. To address this issue, we investigate the edge dependence of the Josephson current in graphene Josephson junctions operating in the quantum Hall regime. By systematically comparing devices with native, etched, edge-free, and gate-defined edges, we demonstrate that the Josephson current is confined to the physical edges and is highly sensitive to specific edge configurations. Our findings provide direct evidence that counter-propagating quantum Hall edge states mediate Andreev bound states, enabling Josephson coupling. These results clarify the underlying mechanism of Josephson current in the quantum Hall regime and offer new strategies for engineering superconducting hybrid devices.

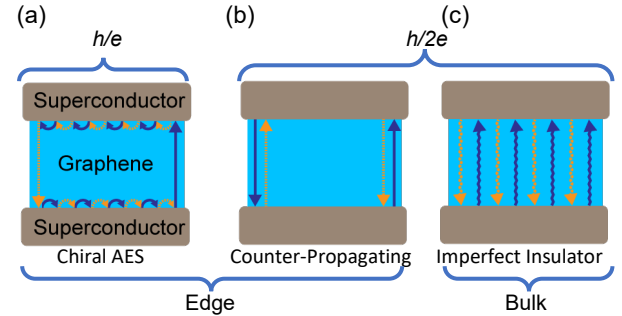
I. INTRODUCTION

Hybrid systems combining superconductivity with topologically nontrivial phases offer a promising route toward realizing Majorana zero modes[1]–[4], a key ingredient for fault-tolerant quantum computing[5]–[7]. Graphene has emerged as a particularly attractive platform for this type of hybridization due to its high-quality interfaces with superconductors[8]–[14] and high electronic quality, enabling the establishment of robust quantum Hall (QH) states[15], [16]. Several noteworthy phenomena have been reported, including the hybridization of superconductivity with integer[17]–[19] and fractional[20] QH states as well as the observation of Josephson coupling[21]–[23] in the QH regime.

The first observation of supercurrent in the QH regime[21] has gained considerable attention because it demonstrates the coexistence of superconductivity which preserves time-reversal symmetry and QH states which require a strong magnetic field. Despite these advances, the mechanism enabling Josephson coupling in the QH regime remains unresolved. A central puzzle lies in the observed magnetic interference patterns with a period of $h/2e$ [21], contrasting with the expected h/e periodicity for chiral Andreev edge states (FIG. 1(a))[22]. Furthermore, deviations of normal-state resistance

from quantized Hall plateaus suggest additional conduction channels that may facilitate supercurrent.

FIG. 1. Schematic representation of the three



potential mechanisms for the formation of Andreev bound states in graphene Josephson junctions (GJJs) operating in the quantum Hall (QH) regime. (a) Chiral Andreev edge states, (b) counter-propagating edge states, and (c) an imperfectly insulating bulk within the QH states. Blue arrows represent electron trajectories, while orange-dashed arrows denote hole trajectories, correlated through Andreev reflections.

Previous studies have proposed that supercurrent is mediated by edge-localized Andreev bound states (ABS). For instance, the weak dependence of supercurrent on the junction width [24] and the ability to control supercurrent using a side gate[25] suggest

*Corresponding author: lghman@postech.ac.kr (G.-H.L.)

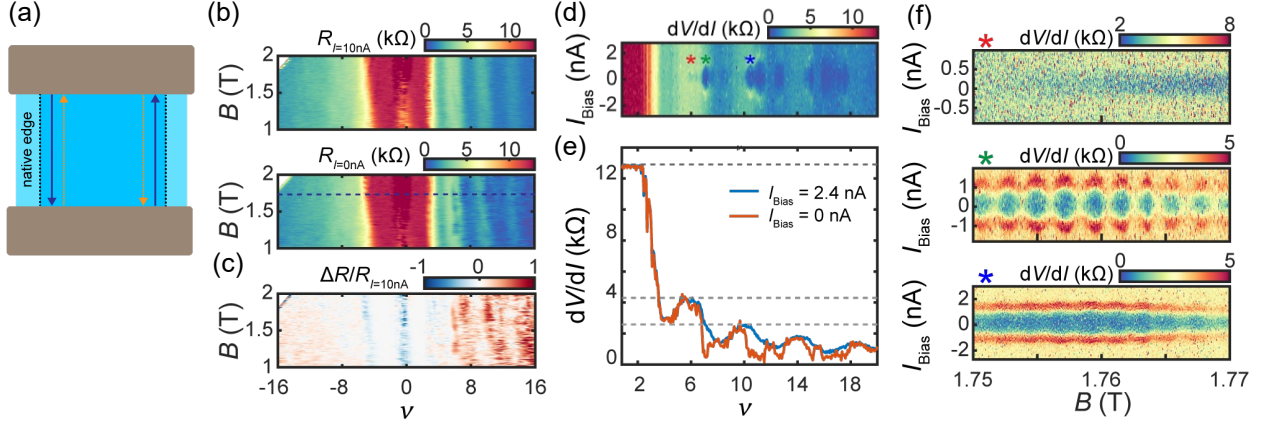


FIG. 2. supercurrent in the quantum Hall regime observed in a graphene Josephson junction (GJJ) with a native edge (NEGJJ-01). (a) Schematic of Andreev bound states formed by counter-propagating edge states in the GJJ. (b) Upper panel: fan diagram of differential resistance measured with a finite direct current (DC) bias of 10 nA ($R_{I=10\text{nA}}$) and with an alternating current excitation of 100 pA. Lower panel: a fan diagram measured without DC bias ($R_{I=0\text{nA}}$). (c) The resistance difference $\Delta R = R_{I=10\text{nA}} - R_{I=0\text{nA}}$ normalized by $R_{I=10\text{nA}}$. (d) The differential resistance (dV/dI) obtained as a function of bias current (I_{Bias}) and filling factor (ν) at a magnetic field of $B = 1.75$ T. (e) dV/dI as a function of ν , measured with and without I_{Bias} . (f) dV/dI as a function of I_{Bias} and B . The upper, middle, and lower panels correspond to $\nu = 5.4, 6.4$, and 9.5 , respectively. Colored symbols correspond to those in the upper panel of (c).

the involvement of counter-propagating edge channels formed near the edge by a non-monotonic carrier density profile (Fig. 1(b)). However, this interpretation remains incomplete as it does not rule out the possibility of bulk-mediated supercurrent, particularly in the filling factor transition regime. Moreover, supercurrent is often observed in regions of imperfect bulk insulation[22][26], raising the question of whether supercurrent can persist even in the absence of well-formed edge states. A closer examination on the previous studies reveals that supercurrent appears predominantly in regions of low normal-state resistance, suggesting that additional conduction channels beyond ideal edge modes may play a role. This ambiguity underscores the need to directly test whether JC can arise in the absence of edge channel conduction.

To address this open question, we systematically investigated the role of edge configurations in mediating supercurrent in GJJs under QH conditions. We examined devices with native, etched, edge-free, and gate-defined boundaries. In an edge-free geometry, which lacks physical edges and supports a single, homogeneous filling factor, we found no evidence of supercurrent even within the filling factor transition regime, thus ruling out bulk-mediated supercurrent under such conditions. Introducing physical edges through etching restores the supercurrent, but the variations in the quality of devices or measurement environments limit a direct comparison. To overcome these limitations, we develop an in-situ geometry that

enables reversible definition of edge channels in the same device and measurement environment. This design allows us to toggle between edge-free and edge-defined configurations without introducing extrinsic differences. Our results show that supercurrent in the transition regime is absent without edge channels and re-emerges only when edges are introduced, providing direct evidence that supercurrent in the QH regime is strictly edge-mediated.

Our work resolves a key ambiguity in previous studies by establishing edge-mediated conduction as a necessary condition for Josephson coupling in GJJs within the QH regime. Moreover, the comparison across different edge configurations points to the existence of counter-propagating edge states that mediate the supercurrent. These findings provide a clear framework for future exploration of hybrid topological superconducting systems and offer guidance for the design of edge-engineered quantum devices.

II. METHODS

We fabricated GJJs with graphene encapsulated in hexagonal boron nitride (hBN)[27], which was stacked on a highly doped silicon (Si) wafer covered with a silicon dioxide (SiO_2) dielectric layer of a thickness of 300 nm. The device geometries and electrodes were defined using electron-beam lithography. Following plasma etching, molybdenum-rhenium (MoRe, 50%/50%) superconducting

*Corresponding author: lghman@postech.ac.kr (G.-H.L.)

electrodes were deposited using direct current sputtering with the same electron beam resist mask to minimize contamination of the exposed graphene edges or surface. We fabricated GJJs with various edge configurations including native edge, etched-edge, edge-free, and graphite gate-defined edge. The etched-edge GJJs were derived from either the native or edge-free GJJs for comparative analyses. The detailed edge configurations and dimensions of the junctions are described in Table S1. All measurements were performed in a dilution refrigerator (Bluefors LD400) with a nominal base temperature of 20 mK, equipped with Thermocoax cables and multistage low-pass and π -filters to minimize unwanted external electrical noise. Measurement details are described in the Supplemental Materials[28].

III. RESULTS

To confirm the quality of the superconducting contacts and the reliability of the measurement system, we reproduced key experimental observations from a previous study[21] using a native edge GJJ (FIG. 2(a)). By comparing the differential resistance measured with and without a DC bias current (I_{Bias}) (FIG. 2(b)), supercurrent regions were visualized using red colors, as shown in the lower panel of FIG. 2(c). These regions were further investigated by varying ν (FIGS. 2(d) and (e)) and B (FIG. 2(f)). In FIG. 2(d), supercurrent pockets appear only for $\nu > 5$, which does not exhibit well-quantized plateaus, suggesting the presence of additional conduction channels beyond the quantum Hall edge states, which host the ABS (FIGS. 1(b) and (c)). The finite differential resistance at zero bias current indicates that the Josephson coupling is easily destabilized by thermal fluctuations due to the small critical current. Nevertheless, the appearance of Shapiro steps under microwave irradiation (FIG. S1) confirms the existence of supercurrent. This result is consistent with the previous study [21], where finite supercurrent was likewise observed near the centers of the $\nu = 6$ and $\nu = 10$ plateaus, although in both cases the quantization is not perfectly ideal.

In FIG. 2(f), the oscillation of critical current (I_c) with B is prominent at $\nu = 6.4$, barely visible at $\nu = 9.5$, and absent at 5.4 while the oscillation period is almost the same as that in the zero-field regime (FIG. S2 (c)), which confirms the oscillation period is $h/2e$, reported in the previous study. This inconsistent behavior can be explained by the counter-propagating edge states scenario depicted in FIG. 1(b). If both edges host supercurrent with similar magnitudes, a SQUID-like interference pattern will emerge, as shown in the case of $\nu = 6.4$. If both edges host supercurrent but with considerably different magnitudes, the interference

results in small oscillation amplitudes with a finite, nonvanishing I_c , as shown in the case of $\nu = 9.5$. If one edge hosts supercurrent while the other does not, no interference occurs, as shown in the case of $\nu = 5.4$.

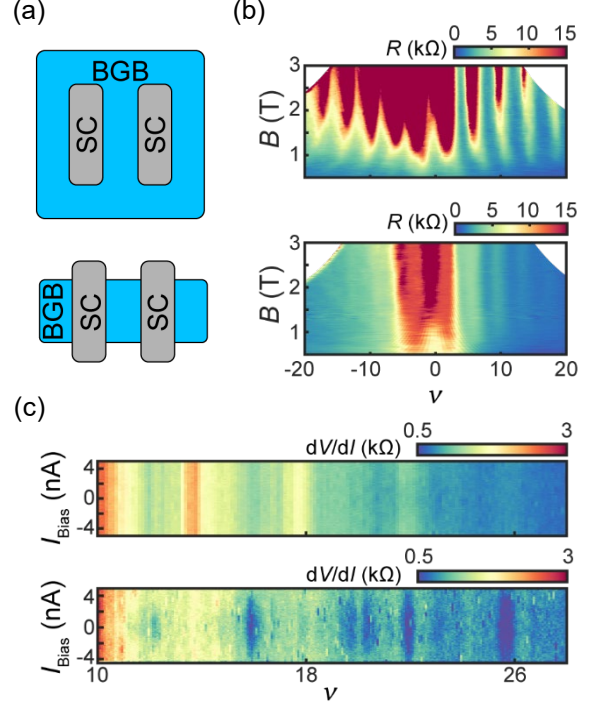


FIG. 3 Josephson current measurement in an edge-free GJJ (EF GJJ-01) and etched-edge GJJ (EE GJJ-01). (a) Schematic of edge-free GJJ (upper panel) and etched-edge GJJ (lower panel). The sky-blue regions represent the hBN/graphene/hBN (BGB) heterostructures. The gray regions correspond to the superconducting electrodes (SC). (b) Fan diagrams of edge-free GJJ (upper) and etched-edge GJJ (lower). (c) Differential resistance as a function of I_{Bias} and ν for edge-free GJJ (upper) and etched-edge GJJ (lower) at magnetic fields of $B = 0.8$ T and 1.3 T, respectively.

For completeness, we note that a conservative bulk picture that treats the residual QH bulk as a uniform diffusive conductor would produce a Fraunhofer-type envelope for the critical current, $I_c(B) = I_{c0}|\sin(\pi\Phi/\Phi_0)/\pi\Phi/\Phi_0|$. Using $I_{c0} \sim 2\mu\text{A}$ and a zero-field period of $\Delta B = 20\text{G}$, this gives $I_c \sim 0.7\text{nA}$ at $B = 1.75\text{T}$, which is comparable to the observed scale. This motivates a direct test of whether the observed supercurrent can be mediated by the bulk.

To validate the counter-propagating edge states scenario (FIG. 1(b)), we examined the edge-free GJJ and etched-edge GJJ devices (FIG. 3(a)) to determine whether the supercurrent in the QH regime was mediated by the bulk of graphene. In the edge-free GJJ

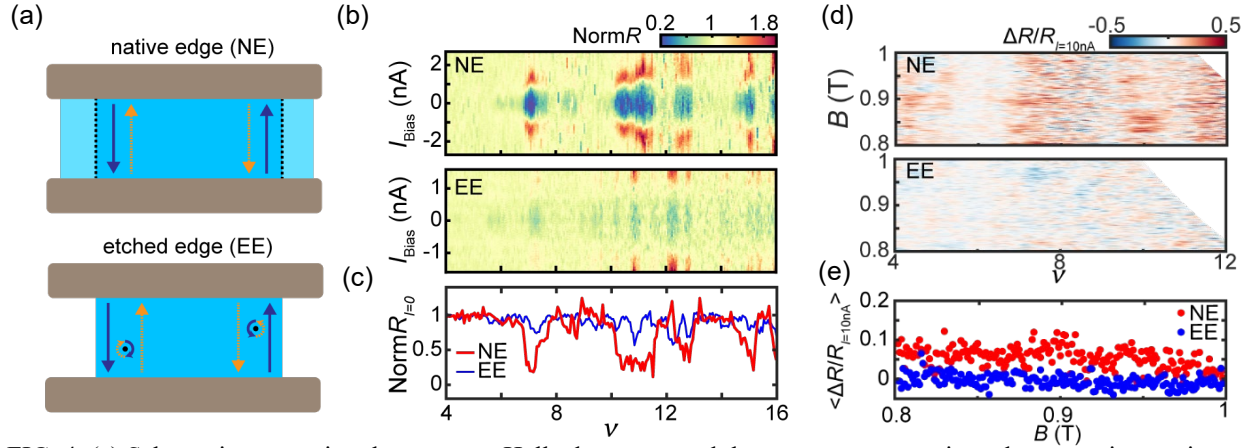


FIG. 4. (a) Schematic comparing the quantum Hall edge states and the counter-propagating edge states in a native edge GJJ and an EE GJJ. (b) Normalized differential resistance ($\text{Norm}R = R_{I=0\text{nA}}/R_{I=10\text{nA}}$) as a function of bias current (I_{Bias}) and filling factor (ν) of a native edge GJJ (NEGJJ-01, upper panel) and etched-edge GJJ (EE GJJ-02, lower panel) at a magnetic field of $B = 1.75$ T. (c) Normalized differential resistance at the zero-bias current $\text{Norm}R_{I=0\text{nA}}$ of native (red curve) and etched (blue curve) edge devices. (d) Fan diagrams of normalized resistance difference ($\Delta R/R_{I=10\text{nA}} = (R_{I=10\text{nA}} - R_{I=0\text{nA}})/R_{I=10\text{nA}}$) of a native edge GJJ (NEGJJ-02, upper panel) and etched-edge GJJ (EEGJJ-03, middle panel). (e) Mean values of horizontal lines in the Fan diagrams of (d) as a function of the magnetic field B .

case, the resistance diverges in the QH regime, as shown in the upper panel of FIG. 3(b), where the longitudinal conductance vanishes. This indicates the absence of edge conduction channels. Consequently, no supercurrents were observed, excluding the possibility that bulk graphene mediates the supercurrent when it is in the plateau transition region[22]. Upon etching, the edge-free GJJ transformed into the etched-edge GJJ, exhibiting supercurrent, as shown in FIG. 3(c), similar to the native edge GJJ in FIG. 2. This abrupt change underscores the necessity of a physical edge for supercurrent, suggesting that ABSs reside at the edge of graphene, thus facilitating the supercurrent.

The existence of counter-propagating edge states seems counter-intuitive because chirality typically forbids backscattering. However, a theoretical prediction suggests that inhomogeneous screening of the electric field by charge carriers in graphene creates a nonmonotonic potential near the edge, facilitating counter-propagating edge states[29]. This phenomenon has been observed in several scanning probe microscopy experiments[30], [31], which revealed that the upstream modes exist several hundred nanometers away from the physical edge. Nonetheless, recent scanning tunneling spectroscopy [32] has demonstrated that QH edge channels in graphene can be tightly confined as ideal 1D chiral states at high magnetic fields ($B=14$ T), with no evidence of electrostatic reconstruction or upstream modes. In contrast, the supercurrent observed in our

GJJ devices appears at much lower magnetic fields ($B < 2$ T), where substantial variations in the local filling factors near the edge can be present so that counter-propagating edge states occur.

In the presence of counter-propagating edge states, the ABS can be formed through Andreev reflection between the downstream and upstream mode at a single edge. However, these ABS can be disrupted by impurities near the edge, which facilitate scattering between the upstream and downstream modes and obstruct ABS formation, as illustrated in FIG. 4(a). The comparison between the native edge GJJ and etched-edge GJJ, as shown in FIG. 4, highlights the detrimental effect of plasma-etching-induced disorder on the formation of Andreev bound states (ABS) [33]. To ensure controlled and direct comparison, measurements were first performed on the device with a native edge GJJ, and the same device was subsequently etched to form an etched-edge GJJ. As shown in FIGS. 4(b) and (c), at a representative magnetic field of 1.75 T, the etched-edge GJJ exhibits a significantly weaker Josephson coupling and a higher normalized differential resistance at zero bias compared to the native edge GJJ. While this single-point comparison indicates suppressed supercurrent in the etched-edge GJJ, it does not reveal whether such suppression persists over a broader range of magnetic fields. To address this, FIG. 4(d) presents fan diagrams for both configurations, capturing the evolution of the normalized resistance difference as a function of magnetic field and filling factor. The overall resistance

*Corresponding author: lghman@postech.ac.kr (G.-H.L.)

difference in the fan diagram is larger for the native edge GJJ, reinforcing the conclusion that the native edge GJJ supports stronger supercurrent across a wider parameter space than the etched-edge GJJ, as illustrated in FIG. 4(e). These results collectively demonstrate that edge disorder introduced by etching inhibits the robust formation of supercurrents mediated by ABS.

This is also supported by observations from a previous scanning probe microscopy study[31], which revealed that the formation of energy levels in the antidots facilitates scattering between the upstream and downstream modes. When more impurities are introduced near the edge through the plasma etching process, the Fermi level can align more frequently, satisfying the conditions for scattering between the upstream and downstream modes. Consequently, the etched-edge GJJ, which has more impurities near the edge compared with the native edge GJJ, experiences more scattering, thereby the supercurrent is suppressed compared with the native edge GJJ.

However, ambiguities remain regarding whether differences in device quality or measurement conditions between the original and etched devices may compromise the fairness of the comparison. To address this issue, we fabricated graphene Josephson junctions on an hBN/graphene/hBN stack, incorporating a narrow graphite strip as a local back-gate to independently tune the filling factor ν_l of graphene in the local region above the graphite. The global filling factor ν_g is controlled separately via the silicon back gate (FIG. 5(a)). We then measured the junctions under various $\nu_l - \nu_g$ configurations (FIG. 5(b)).

When ν_l equals ν_g , the two superconducting electrodes are connected only through longitudinal conduction, which vanishes due to the edge-free geometry (FIG. 5(c) and FIG. S3 (a)). The absence of supercurrent in this configuration further supports that supercurrent is not mediated by the bulk of quantum Hall graphene at any filling factor (FIG. 5(d)).

Moreover, the dependence of supercurrent on ν_l and ν_g provides insights into the mechanism underlying the formation of Andreev bound states (ABS). The supercurrent pockets, shown in red in FIG. 5(d), appear in the regions corresponding to Configurations 2 and 3 in FIG. 5(b), but are absent in Configuration 1. As illustrated in FIG. 5(b), when $|\nu_g|$ is greater than $|\nu_l|$ and the two share the same sign, as in Configuration 1, the net downstream modes in the global region propagate in the same direction as the upstream mode in the local region. This results in the absence of counter-propagating edge states and prevents the formation of ABS. In Configurations 2 and 3, upstream and downstream modes coexist and

form counter-propagating pairs, which can support ABS. This interpretation, based on the counter-propagating edge state framework, is consistent with the experimental observations in FIGS. 5(c) and 5(d), where supercurrent is absent in Configuration 1 and clearly present in Configurations 2 and 3.

IV. DISCUSSION

Our measurements indicate that supercurrent is confined to the graphite-gated side. The supercurrent pockets in FIG. 5(d) appear as vertical stripes versus ν_l , which show that ABS and associated upstream modes are confined to the locally gated region. Finite-element electrostatics in Fig. S4 show that the carrier-density gradient at the graphite edge is much sharper than at the Si-gated edge because the graphite gate lies much closer to graphene. Such an abrupt edge profile can induce a non-monotonic dispersion that supports upstream mode[29] only on the local graphite-gated side, whereas the smoother global Si-gated side does not reach this regime. In this situation, the upstream mode pairs with the net downstream mode to form counter-propagating edge states at graphite-gated side at the boundary. These states establish ABS and enable observed supercurrent. This picture explains the presence of supercurrent in Configurations 2 and 3 and its absence in Configuration 1.

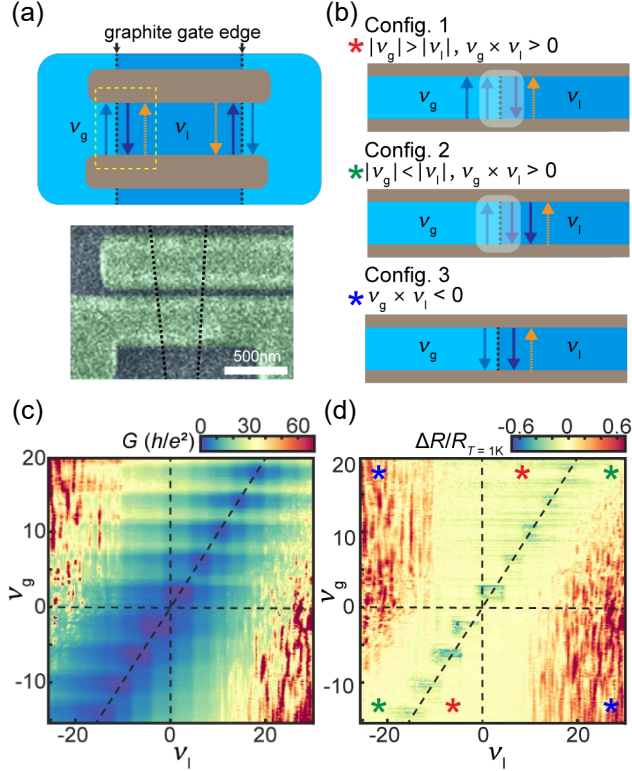
V. CONCLUSIONS

GJJs with various edge configurations were fabricated and analyzed to investigate the mechanisms governing ABS formation in the QH regime. All experimental observations consistently supported the counter-propagating edge states scenario, in which Andreev coupling between the upstream and downstream modes accounted for the observed supercurrent in the QH regime. These findings provide a clearer understanding of how GJJs can sustain supercurrent in the QH regime and highlight the importance of considering upstream modes when designing graphene-based QH devices.

Our work suggests that counter-propagating edge states can be further engineered to facilitate the hybridization of superconductivity with QH states by precisely controlling the edge potential, for example, through side or graphite gates. Furthermore, introducing spin polarization in counter-propagating edge states could provide a promising route toward realizing Majorana zero modes when combined with superconductivity.

FIG. 5 (a) Upper panel shows a quasi-classical schematic of the graphite gate-defined edge graphene

*Corresponding author: lghman@postech.ac.kr (G.-H.L.)



Josephson junction. The lower panel shows a scanning electron microscopy image of GGDEGJJ-01. Dashed lines indicate the edge of the graphite gate beneath the hexagonal boron nitride (hBN)/graphene/hBN stack. The green-colored region indicates the superconducting electrodes. (b) Schematic illustrating the upstream and downstream modes of local and global region for three possible configurations, namely 1, 2, and 3. Arrows with blue, indigo, and orange colors indicate the downstream mode in the global region, that in the local region, and the upstream mode in the local region, respectively. Shading incorporating blue and indigo arrows indicates the mixing of downstream mode in the local and global regions. (c) Conductance G as a function of the filling factor for the local and global regions ν_l and ν_g , respectively, measured with an AC excitation current of 1 nA at a magnetic field of $B = 3.1$ T. (d) Normalized resistance difference obtained as a function of ν_l and ν_g . Dashed lines divide the plot into three regions corresponding to the configurations illustrated in (b).

ACKNOWLEDGMENTS

This work was supported by National Research Foundation (NRF) Grants (Nos. RS-2022-NR068223, RS-2024-00393599, RS-2024-00442710, RS-2024-00444725, 2022R1A6A3A01086903) and ITRC program (IITP-2025-RS-2022-00164799) funded by the Ministry of Science and ICT, Samsung Science

and Technology Foundation (Nos. SSTF-BA2401-03 and SSTF-BA2101-06), and Samsung Electronics Co., Ltd. (IO201207-07801-01).

To whom all correspondence should be addressed: lghman@postech.ac.kr.

- [1] Fu, L., and C.L. Kane, Phys. Rev. B **79**, 161408, (2009).
- [2] Qi, X.L., and S.C. Zhang, Rev. Mod. Phys. **83**, 1057, (2011).
- [3] Lindner, N.H., E. Berg, G. Refael, and A. Stern, Phys. Rev. X **2**, 041002, (2012).
- [4] Clarke, D.J., J. Alicea, and K. Shtengel, Nat. Commun. **4**, 1348, (2013).
- [5] Kitaev, A.Y., Ann. Phys. (N. Y.) **303**, 2, (2003).
- [6] Nayak, C., S.H. Simon, A. Stern, M. Freedman, and S. Das Sarma, Rev. Mod. Phys. **80**, 1083, (2008).
- [7] Sarma, S. Das, M. Freedman, and C. Nayak, npj Quantum Inf. **1**, 15001, (2015).
- [8] Heersche, H.B., P. Jarillo-Herrero, J.B. Oostinga, L.M.K. Vandersypen, and A.F. Morpurgo, Nature **446**, 56, (2007).
- [9] Mizuno, N., B. Nielsen, and X. Du, Nat. Commun. **4**, 2716, (2013).
- [10] Calado, V.E., S. Goswami, G. Nanda, M. Diez, A.R. Akhmerov, K. Watanabe, T. Taniguchi, T.M. Klapwijk, and L.M.K. Vandersypen, Nat. Nanotechnol. **10**, 761, (2015).
- [11] Ben Shalom, M., M.J. Zhu, V.I. Fal'ko, A. Mishchenko, A. V. Kretinin, K.S. Novoselov, C.R. Woods, K. Watanabe, T. Taniguchi, A.K. Geim, et al., Nat. Phys. **12**, 318, (2016).
- [12] Borzenets, I. V., F. Amet, C.T. Ke, A.W. Draelos, M.T. Wei, A. Serebinski, K. Watanabe, T. Taniguchi, Y. Bomze, M. Yamamoto, et al., Phys. Rev. Lett. **117**, 237002, (2016).
- [13] Park, J., J.H. Lee, G.H. Lee, Y. Takane, K.I. Imura, T. Taniguchi, K. Watanabe, and H.J. Lee, Phys. Rev. Lett. **120**, 77701, (2018).
- [14] Schmidt, F.E., M.D. Jenkins, K. Watanabe, T. Taniguchi, and G.A. Steele, Nat. Commun. **9**, 4069, (2018).
- [15] Bolotin, K.I., F. Ghahari, M.D. Shulman, H.L. Stormer, and P. Kim, Nature **462**, 196, (2009).
- [16] Dean, C.R., A.F. Young, I. Meric, C. Lee, L. Wang, S. Sorgenfrei, K. Watanabe, T. Taniguchi, P. Kim, K.L. Shepard, et al., Nat. Nanotechnol. **5**, 722, (2010).
- [17] Rickhaus, P., M. Weiss, L. Marot, and C. Schönenberger, Nano Lett. **12**, 1942, (2012).

- [18] Lee, G.H., K.F. Huang, D.K. Efetov, D.S. Wei, S. Hart, T. Taniguchi, K. Watanabe, A. Yacoby, and P. Kim, *Nat. Phys.* **13** , 693, (2017).
- [19] Park, G.H., M. Kim, K. Watanabe, T. Taniguchi, and H.J. Lee, *Sci. Rep.* **7** , 10953, (2017).
- [20] Gül, Ö., Y. Ronen, S.Y. Lee, H. Shapourian, J. Zauberman, Y.H. Lee, K. Watanabe, T. Taniguchi, A. Vishwanath, A. Yacoby, et al., *Phys. Rev. X* **12** , 021057, (2022).
- [21] Amet, F., C.T. Ke, I. V. Borzenets, J. Wang, K. Watanabe, T. Taniguchi, R.S. Deacon, M. Yamamoto, Y. Bomze, S. Tarucha, et al., *Science* (80-.). **352** , 966, (2016).
- [22] Vignaud, H., D. Perconte, W. Yang, B. Kousar, E. Wagner, F. Gay, K. Watanabe, T. Taniguchi, H. Courtois, Z. Han, et al., *Nature* **624** , 545, (2023).
- [23] Barrier, J., M. Kim, R.K. Kumar, N. Xin, P. Kumaravadivel, L. Hague, E. Nguyen, A.I. Berdyugin, C. Moulds, V. V. Enaldiev, et al., *Nature* **628** , 741, (2024).
- [24] Draelos, A.W., M.T. Wei, A. Seredinski, C.T. Ke, Y. Mehta, R. Chamberlain, K. Watanabe, T. Taniguchi, M. Yamamoto, S. Tarucha, et al., *J. Low Temp. Phys.* **191** , 288, (2018).
- [25] Seredinski, A., A.W. Draelos, E.G. Arnault, M.T. Wei, H. Li, T. Fleaaming, K. Watanabe, T. Taniguchi, F. Amet, and G. Finkelstein, *Sci. Adv.* **5** , eaaw8693, (2019).
- [26] Wei, M.T., A.W. Draelos, A. Seredinski, C.T. Ke, H. Li, Y. Mehta, K. Watanabe, T. Taniguchi, M. Yamamoto, S. Tarucha, et al., *Phys. Rev. B* **100** , 121403, (2019).
- [27] Wang, L., I. Meric, P.Y. Huang, Q. Gao, Y. Gao, H. Tran, T. Taniguchi, K. Watanabe, L.M. Campos, D.A. Muller, et al., *Science* **342** , 614, (2013).
- [28] See Supplemental Material at <http://link.aps.org/> which includes the details on device information, additional data and numerical simulations.
- [29] Silvestrov, P.G., and K.B. Efetov, *Phys. Rev. B* **77** , 155436, (2008).
- [30] Marguerite, A., J. Birkbeck, A. Aharon-Steinberg, D. Halbertal, K. Bagani, I. Marcus, Y. Myasoedov, A.K. Geim, D.J. Perello, and E. Zeldov, *Nature* **575** , 628, (2019).
- [31] Moreau, N., B. Brun, S. Somanchi, K. Watanabe, T. Taniguchi, C. Stampfer, and B. Hackens, *Nat. Commun.* **12** , 4265, (2021).
- [32] Coissard, A., A.G. Grushin, C. Repellin, L. Veyrat, K. Watanabe, T. Taniguchi, F. Gay, H. Courtois, H. Sellier, and B. Sacépé, *Sci. Adv.* **9** , eadf7220, (2023).
- [33] Jeong, H.W., S. Jang, S. Park, K. Watanabe, T. Taniguchi, and G.H. Lee, *Nano Lett.* **24** , 15950, (2024).